Introducing a novel gravitation-based high-velocity compaction analysis method for pharmaceutical powders

Tanner, Timo

2017-06-30

Tanner , T , Antikainen , O , Ehlers , H & Yliruusi , J 2017 , ' Introducing a novel gravitation-based high-velocity compaction analysis method for pharmaceutical powders ' , International Journal of Pharmaceutics , vol. 526 , no. 1-2 , pp. 31-40 . https://doi.org/10.1016/j.ijpharm.2017.04.039

http://hdl.handle.net/10138/308430
https://doi.org/10.1016/j.ijpharm.2017.04.039

Introducing a novel gravitation-based high-velocity compaction analysis method for pharmaceutical powders

Timo Tanner[a], Osmo Antikainen[a], Henrik Ehlers[a], Jouko Yliruusi[a]

[a]*Division of Pharmaceutical Chemistry and Technology, Faculty of Pharmacy, University of Helsinki. P.O.Box 56 (Viikinkaari 5E), FIN-00014 University of Helsinki, Finland*

Abstract

With modern tableting machines large amounts of tablets are produced with high output. Consequently, methods to examine powder compression in a high-velocity setting are in demand. In the present study, a novel gravitation-based method was developed to examine powder compression. A steel bar is dropped on a punch to compress microcrystalline cellulose and starch samples inside the die. The distance of the bar is being read by a high-accuracy laser displacement sensor which provides a reliable distance-time plot for the bar movement. In-die height and density of the compact can be seen directly from this data, which can be examined further to obtain information on velocity, acceleration and energy distribution during compression. The energy consumed in compact formation could also be seen. Despite the high vertical compression speed, the method was proven to be cost-efficient, accurate and reproducible.

Keywords: tabletting, compaction, compression, viscoelasticity, microcrystalline cellulose, starch

Chemical compounds studied in this article

Microcrystalline cellulose (PubChem CID: 62698); Amioca (PubChem CID: 86278134)

*Corresponding author: Timo Tanner (M.Sc.), Division of Pharmaceutical Chemistry and Technology, Faculty of Pharmacy, University of Helsinki. P.O.Box 56 (Viikinkaari 5E), FIN-00014 University of Helsinki, Finland. Tel. +358249159158. Fax +358 294159138. E-mail timo.tanner@alumni.helsinki.fi

1. INTRODUCTION

1.1. Background

Understanding powder compression behavior is crucial when designing a tablet formulation. During tableting, when powder is compressed between punches, particles rearrange, fragment and deform under pressure resulting in a volume decrease and compact formation (Adolfsson & Nyström 1996; Antikainen & Yliruusi 2003; Hiestand et al. 1977; Zhang et al. 2003). As deformed particles are forced to pack into a smaller volume, new bonds are formed. Bonding occurs mostly due to Van der Waals interaction, electrostatic interaction, hydrogen bonding, local melting and mechanical interlocking. Perfectly plastic behavior refers to a phenomenon where this bonding allows the particle to retain its new shape whereas perfectly elastic particles do not create new bonds, causing the particle to recover to its original shape. Fragmentation refers to a phenomenon where particles break under pressure forming smaller particles, which can further rearrange and fill the voids between the larger particles. Plastic deformation is a time-dependent phenomenon whereas fragmentation occurs immediately when enough pressure has been applied.

Most materials are viscoelastic in nature and compression behavior of any material is a mixture of plastic deformation, elastic deformation and fragmentation. It is of importance to understand that the fraction of each phenomenon is condition-dependent meaning that, for instance, any material can presumably resist plastic flow if the compression speed is high enough (Tatavarti et al. 2008; Thoorens et al. 2014). Many other factors, for instance, compression pressure, humidity, temperature and particle surface characteristics in general may affect these phenomena as well (Amidon & Houghton 1995; Nokhodchi 2005; Rouèche et al. 2006). In a typical tableting setting microcrystalline cellulose (MCC) is dominantly known as a plastic material, starch as an elastic material and dicalcium phosphate as a fragmenting material, to name a few (Antikainen & Yliruusi 2003; Shlieout et al.2002). However, such categorization is not unambiguous and the compression behavior varies depending on conditions.

1.2. Importance of compression behavior

Compacts consisting mostly of plastically deforming particles have a high probability of showing excessive hardness and possibly poor disintegration after administration. In contrast, pronounced elasticity promotes formation of weaker tablets or complete failure to form compacts (Hiestand et al. 1977; Katz et al. 2013). Tablet defects such as lamination or capping may also occur if the excipients are imbalanced in a formulation with regard to their properties (Tatavarti et al. 2008). Therefore, it is important to know the compression behavior of the individual components and the powder blend when designing a feasible formulation. A tablet should be hard enough to withstand the manufacturing and storage conditions and yet weak enough to disintegrate allowing the active ingredient to dissolve and absorb inside the GI-tract. Furthermore, it is crucial to remember that compression behavior alone does not dictate the properties of the compact, as each material contributes to the formulation with unique functional features such as disintegrating or binding effect.

1.3. Compaction simulators

Powder compaction simulators have been designed to assist in designing a tablet formulation. They are typically hydraulic or mechanically powered and are constructed to mimic the stages of tableting while consuming only minuscule amounts of material compared to common tableting processes (Michaut et al. 2010; Rees et al. 1972). Hydraulic machines tend to resemble eccentric tableting machines and mechanical machines mimic rotary tableting machines even though often being linear in design. At their best, compaction simulators can mimic all of the events of a tableting process ranging from die-filling to ejection and can be very useful tools in pharmaceutical formulation design. The main problem in utilizing some of the commercially available compaction simulators seems to be that a certain simulator may have to be paired with a certain tableting machine to get comparable results. Therefore, setting up the machines and testing them in various conditions to ensure comparable results may require extensive effort, as aptly demonstrated by Neuhaus (2007). Modern simulators are more user-friendly but the cost of these machines is still high.

1.4. Gravitation based high-velocity compaction analysis

In the present study, a gravitation-based high-velocity compaction analysis method is presented. A novel device was constructed to provide accurate information about powder compression. The device differs from current tableting machines and compaction simulators as it does not force the powder into a specified volume, but allows the powder to freely resist compression. Therefore, the properties of powder ultimately determine the maximum compression pressure. This enables acquiring pure substance or blend specific compression profiles. Tableting events other than compression itself, such as die-filling and ejection, are deliberately ignored in this setting in order to focus on compression and maintain the simplicity of the device. Thus, the device has not been constructed to replace a tableting simulator but to provide additional information about powder behaviour. All data obtained with the method is based on measuring distance as a function of time, and the basic physics accompanied is uncomplicated. The cost of the device is roughly 20 000 USD.

First, introductory testing was carried out to prove the accuracy of the setup. Following this, samples of MCC and starch were compressed consecutively to obtain compressibility profiles and energy distribution data. In the present study, we sought to prove that the presented method is valid for powder compression examination in an accurate and reproducible manner. Furthermore, we wanted to show that distance measurement with a known sampling frequency is the only requirement to derive information about the compression event.

2. MATERIALS AND METHODS

2.1. Materials

Powder compression studies were performed on microcrystalline cellulose (Avicel PH-102; FMC BioPolymer; Lot 7314C) and starch (Amioca powder TF; National Starch; Lot CGH-358/0439). The die walls and punches were lubricated using 5 % w/w magnesium stearate (Ph. Eur) in acetone (technical grade).

2.2. Sample preparation

All samples were individually weighed using an analytical balance (Table 1). The water activity of the samples was measured with a water activity meter (AquaLab Series 3, Decagon Devices Inc., Pullman, Washington, USA) and the ambient room temperature and relative humidity were measured with a moisture tester (Mastech MS6900, Precision Mastech, City of Industry, California, USA). The height of the powder bed in the die before compression was derived from time-distance data recorded during compression.

Table 1: Sample and compact characteristics (average ± standard deviation; n=3).

2.3. High-speed gravitational compression device

2.3.1. Structure and function of the device

In the present study, a novel device was constructed to analyze the event of powder compression and compression properties of substances (Figure 1). The device consists of a cylindrical steel bar with a length of 1 m and total mass of 6.27 kg mounted to a rigid frame. The bar is mounted onto a partially Teflon coated frame using Teflon coated bearings and extension pieces to restrict torsional and rotational motion, which combined result in nearly frictionless and strictly vertical motion of the bar. The bar is dropped from a controlled height of 0-200 mm onto an 18 mm high, circular flat faced punch with a diameter of 8 mm and corresponding die with a combined mass of 2.71 kg mounted on a steel anvil with a mass of 49.0 kg. The die consists of three different parts and can be dismantled to remove the compact after compression. The anvil is connected to an 11.5 kg concrete brick through 4 attachment pins. Rubber sheets are placed between the anvil and concrete brick and between the concrete brick and the ground to reduce horizontal motion of the device during impact. The anvil is made of decarbonized steel and all other metal parts are made of hardened steel (HRC 60-64). Decarbonized steel is relatively soft which ensures that the base deformation can be clearly detected.

Fig 1: Schematic representation of the gravitational high-speed compression device. A) Adjustment bolt; B) Magnet; C) Power supply; D) Falling height scale; E) Upper extension piece; F) Bar; G) Bearings; H) Main frame; I) Lower extension piece; J) Punch and die; K) Bar distance sensor and laser; L) Base distance sensor and laser; M) Anvil; N) Rubber sheets; O) Attachment pin; P) Concrete brick; Q) Data acquisition controller; R) Laptop; S) Safety latch.

2.3.2 Data acquisition

Two high-accuracy laser displacement sensors were used (Keyence LK-H087, Keyence Corporation of America, Itasca, Illinois, USA) to measure displacement of the bar and the base as a function of time. The displacement of the bar was measured from the lower extension piece (Figure 1-I) and the displacement of the base was measured from the top surface of the anvil. The lasers were connected by cables to a controller (Keyence-G5001P, Keyence Corporation of America, Itasca, Illinois, USA), which was further connected to a DC power supply providing a voltage of 24 V (TTI EX752M, AimTTi, Cambridgeshire, UK) and a laptop computer. Time and distance data was recorded using Keyence LK_H3 –software (Keyence Corporation of America, Itasca, Illinois, USA). The detection resolution was 1 µm, sampling rate was 20 kHz and the laser range was set at 36 mm.

To obtain the velocity and acceleration data, the time-distance data was processed mainly using Savitzky-Golay filtering in MATLAB (Version 2014b, Mathworks Inc, Natick, Massachusetts, USA). Time-distance data was first processed with quadratic polynomial and a window size of 7. Velocity data was derived from this data with a 6-degree polynomial and a window size of 101. Acceleration data was derived from this data with a quadratic polynomial and a window size of 11. In this paper, all time-distance data presented is unfiltered as the filtering was made only to obtain the further derivations reliably.

2.3.3. Principle of measurement

The powder compression data acquired with the method is refined from data on distance as a function of time. The first derivative provides a velocity function and the second derivative an acceleration function, from which various parameters can be calculated. For instance, velocity data can be used to

calculate kinetic energy and force on impact can be calculated from acceleration data. Distance data alone could also reveal some mechanic properties of a material.

A full compression event cycle is completed as follows. The device is prepared for measurement first by setting the zero point for distance when the bar is resting on the punch placed in the empty die (Figure 1). Consequently, the lower-most position of the upper punch is known and the distance acquired during measurement describes in-die-height of the powder/compact during contact with the punch. The die is filled with a known amount of powder and the punch is carefully set into the die resting on top of the powder. Lubrication of the die (5 % w/w magnesium stearate in acetone applied with a brush) can be done before filling in the ingredient(s). The falling height is then determined by using the scale located on the upper part of the frame. Upon completion of the preparation, the safety latch is opened and the bar is lowered to the initial falling height position, while only being held in place by the magnet.

A complete compression cycle is presented in Figure 2. First, the power supply is turned on, consequently turning off the magnet, which results in the bar being released. The following acceleration of the bar is approximately 9.7 m/s^2. Upon contact with the powder in the die (dashed line in Figure 2), the bar starts to decelerate. When the powder has been compressed into its smallest volume after impact, the point of maximum displacement has been reached. At this moment, the velocity of the bar is zero, and attains opposite values upon changing direction following maximum displacement. When the bar reaches a second impact, the compact is already undergoing elastic recovery, and as the new collision occurs the bar is sent back up again. This can be seen in the Figure 2 as stages 2 and 3 repeat several times. In Figure 2 three notable collisions between the bar and the powder/compact have occurred allowing elastic recovery to be roughly estimated through these points. As the compaction ends, the final displacement level depicts the in-die height of the compact.

Fig 2: Stages of powder compaction with the method.

The falling height determines the maximum velocity before contact with the punch and is thus based on elementary physics. For example, a falling height of 50 millimeters produces a maximum velocity of roughly 1 m/s. From this acceleration on impact and thus the impact force can be calculated. It is also of importance to understand that the distance data depicts the movement of the bar and not the punch as these two are not attached to each other and in terms of compact formation the bar is specifically used to deliver the energy onto the punch. However, these two are in contact during crucial moments such as the maximum displacement-point and the final displacement-level.

2.3.4. Base movement

Monitoring the movement of the base is a prerequisite for calculating the energy spent on bond formation in the compact correctly. Due to technical reasons the sensor reading the base location was not located directly under the bar, which caused a delay of approximately 0.5 ms in the base movement reading after the impact. Nevertheless, even if the sensor was located at the center, the base would be set in motion with a small delay after impact due to the deformation wave having to reach the base after having left the die.

2.3.5. Energy calculation

The total energy and how the energy is distributed is fundamental knowledge when analyzing the compression event. The initial potential energy is the total energy of the system. Elevating the bar further equals higher potential energy and thus higher total energy. After collision, most of the energy is distributed into upward motion of the bar resulting in gain of potential energy, compact formation, downward motion of the base, deformation of the affected parts of the device, friction, released heat and sound.

When powder is being compressed the total amount of non-elastic work can be read from upward motion of the bar after collision. This work is equal to the change in potential energy between the starting point of the bar and the highest point reached after impact (ΔE). This information alone does not reveal the amount of energy spent on compact formation, however, since some of this energy is

lost on other non-elastic work as well. By operating the device without any powder in the die an estimation of this energy loss could be made (Figure 3 & 4).

Fig 3: Bar and base movement when operating the device without powder with a falling height of 10 millimeters. The change of potential energy, ΔE, can be directly calculated from distance data.

The energy loss for each collision was approximately 60%. It was found that there was a correlation between lost potential energy and the velocity of the base after impact when the bar was dropped from different heights. Consequently, the amount of lost energy even with powder in the die could be calculated by monitoring the base movement.

Fig 4: Plot depicting energy loss during compression (n=3)

As seen in Figure 2, even when there is powder in the die, the springback for the bar can be measured after the first impact, which reveals the total potential energy loss or in other words the total amount of non-elastic work. The amount of energy loss on impact is then calculated using the equation shown in Figure 4 and, along with the potential energy gained by immediate compact recovery, subtracted from the total amount of non-elastic work. The result is the amount of energy spent on compact formation, or to be exact, the total internal energy of the compact immediately after the compression. It must be noted that calculating only the kinetic energy of the base, instead of utilizing the correlation method described above, would cause errors as long as the spring constant of the system remained unknown. One could imagine that as the heavy anvil rested on soft rubber sheets, a concrete block and the floor, the whole system was like a partially compressed spring. Furthermore, different parts of the system, especially the bar and the punch, could be regarded as springs. Since the base consisted of several different objects it was decided that determining a spring constant would have been too complicated and the described correlation was utilized instead. Some errors are present in correlation

as well since one could assume that the relative amount of heat, sound and plastic deformation of the machine parts are dependent on whether there is powder in the die or not.

2.4. Compression studies

To ensure the repeatability of the machine and reliability of the data, experiments were carried out without any powder in the die. These results were used to determine the correlation between base movement and the amount of energy lost during impact. The bar was dropped from five different heights: 10 mm, 20 mm, 30 mm, 40 mm and 50 mm, all in triplicate. After that, samples of MCC (Avicel PH-102) and starch (Amioca powder TF) were compressed five times consecutively with a falling height of 40 mm. The experiments were performed in triplicate.

3. RESULTS AND DISCUSSION

Before engaging in experiments on pharmaceutical powders, the device was operated empty to ensure the conservation of mechanical energy and assess the repeatability of the device in operation. Data on distance as a function of time was acquired from five initial heights, and the zero point of distance was set at the bottom of the die before impact, in order to visualize the non-elastic deformation of the system. In Figure 5 the deformation can be seen as the reading goes below the zero point which was set at the bottom of the die. It is of importance to understand that the base deformation is a complicated system consisting of different parts and the immediate deformation seen here is most likely that of the punch since it is the uppermost part of the base and collides with the falling bar. The base movement can be seen 0.5 ms after the impact but it still takes roughly 10 ms for the bottom of the deformation wave (or maximum displacement of the base) to reach the point where the base is being read by the sensor. The asymmetrical shape of the parabola indicates a non-elastic collision, as some of the energy is transferred into base motion. Within a set of three drops from the same height the largest deviation in maximum displacement point was ±12 micrometers proving the measurement systems to have been reasonably accurate.

Fig 5: Distance data of five drops without any powder in the die

In terms of distance data accuracy, the machine was not completely robust. After the impact, vibrations affected the measurement outcome as the lower extension piece, from which distance data was being read, showed distinct vibration. The bar was one meter in length and thus the mass, or masses of the molecule layers in the bar, accumulated during impact which caused vibration as molecules in the bar were moving to different directions causing the extension piece to vibrate as well. Theoretically, the speed of sound in steel is approximately 6000 m/s so it would take approximately 1/3 of a millisecond for the deformation wave to pass the extension piece, on its way up and down along the one-meter long bar. In Figure 6A there is no powder in the die and the vibration can be clearly seen. When powder has been added, the vibration is present but is weaker in magnitude as seen in Figure 6B. In Figure 6C the vibrations of each of these cases have been isolated by subtracting the original values from their trendline, showing the significant difference in the magnitude of vibration. Three notable waves occur during one millisecond which is close to theorized value of the speed of sound in steel. This finding emphasizes the importance of a sufficiently large sampling frequency, exceeding that needed for being able to detect only the external motion of the bar.

Stoianovici and Hurmuzlu (1996) found that when a steel bar with a length of 600 mm was dropped onto a massive surface causing a centrally positioned collision, 3% of the initial kinetic energy was stored in the steel bar as longitudinal vibrations, and 25% of the energy was dissipated through surface damping and friction, or local deformation following impact. In the present study, vibration of the steel bar was detected upon experiments with an empty die, whereas when there was powder in the die the vibrations were significantly smaller and hardly measurable, having a peak-to-peak amplitude of approximately 1 μm or less. Thus, it can be concluded that no considerable amount of energy was lost due to longitudinal vibration when studying powders, and the kinetic energy directed to the powder was consumed into rearrangement and deformation of the powder bed and setting the

base in motion. In the present study, bending and rotational vibrations were structurally prevented, and thus the effects of longitudinal vibrations only need to be taken into account. Stoianovici and Hurmuzlu (1996) showed that small variations in drop angle did not change the coefficient of restitution of a dropping steel bar to any major extent. They also showed that in centrally positioned impacts the collision is singular. Although some small variation could be expected in the drop angle, one can assume that the impacts in the present study were centrally positioned single impacts. Running the machine without powder is not necessary after acquiring the energy correlation equation so it can be regarded as a special case. However, the phenomenon must be acknowledged since the amount of vibration is dependent on type of material being compressed and the falling height of the bar. During consecutive compressions, the magnitude of vibration also logically increases as the powder/compact hardens and the force on impact increases.

Fig 6: Notable vibration in the extension piece as the bar moves back up after the impact.

Distance-time data was derived further to obtain various information (Figure 7). The data in the distance-time plots was unfiltered (A-B). Energy, speed, acceleration and force-displacement plots (C-F) were processed with Savitzky-Golay-filtering. Vibrations after the impact, as shown in Figure 6, are also visible here, especially in the plot describing the speed of the bar as a function of time (Figure 7D). In the plot describing energy as a function of time (Figure 7C) the total energy does not remain entirely constant before the impact, which shows that the system was not completely free of friction. This might explain the deviation of the measured falling acceleration (9.7 m/s^2) in comparison to gravitational acceleration (9.81 m/s^2). In the energy plot, the total energy converts to non-elastic energy and residual potential energy can still be seen as the compact recovery occurs after the compression.

Fig 7: Compression data of starch: A) Distance-time near maximum displacement; B) Contact time (first contact at zero); C) Energy distribution; D) Bar and base speed; E) Acceleration during impact; F) Force-displacement during impact

When compressing powders the initial powder bed height was approximately 7.8 mm for MCC and 5.7 mm for starch resulting in slightly higher maximum velocity for the first compression in starch compared to MCC. The exact powder bed height can be seen as the change in the bar acceleration as it starts to decelerate immediately after the first contact with the punch. Plots consisting of maximum displacement points and final displacement levels can be seen in Figure 8 where y-axis shows relative volume of the powder/compact. The volumes were normalized based on the initial height of the powder bed, resulting in obtaining unity before compression and lower values after compression. Again, maximum displacement point was the point when the powder was compressed into its minimum volume and final displacement was the in-die-height of the powder/compact after the compression. The corresponding powder bed densities are shown in Figure 9. Maximum density refers to the density at the point of maximum displacement and final density refers to final in-die powder/compact density after each compression. The relative standard deviations in both Figure 8 and 9 were below 2 %, rendering the error bars non-detectable in the graph. This was interpreted as further evidence of the systematic behavior of the measurement device.

Fig 8: Relative volume reduction after five consecutive compressions of MCC and starch (n=3, RSD<2%)

Fig 9: Changes in MCC and starch density after five consecutive compressions (n=3, RSD<2%)

When compressing powders consecutively five times, the changes in relative volume instantly revealed different powder compression behaviour between MCC and starch. After five compressions MCC lost approximately 60% of its original volume whereas volume loss of starch was only 40%. Furthermore, after the compressions 2-5, MCC still lost one third of its volume whereas the

corresponding volume loss for starch was roughly 15%. The distance between the maximum and final points depicts compact recovery, which, after first compression, was roughly 10% for MCC and 14% for starch when compared to final compact height. These values exactly match those reported by Haware et al. 2010. Together these findings support the current knowledge of MCC having superior compressibility between the two (Shlieout et al.2002; Thoorens et al. 2014). Even though the volume loss in starch compact is lower and elastic recovery higher, it would appear that both excipients deform plastically to some degree, MCC more than starch. One could assume that there would be no further volume loss after first compression if the sample was completely elastic, since it was already in compact form. During first compression, on the other hand, particles can rearrange and fragment which means that volume loss can always be seen (assuming that bulk density<<tapped density<<true density). Higher elasticity promotes weaker tablets and higher plasticity harder tablets (Hiestand et al. 1977). These graphs could assist in finding the most optimal compressibility for the formulation. Density plots show that MCC had initially lower bulk density compared to starch but after the compressions the MCC compacts were denser than the starch compacts. Again, the distance between the plots of each material depicts elasticity which was significantly greater in starch compact.

A certain curious phenomenon can be seen in Figure 2 when powder is being compressed. After the second impact, the springback for the bar was actually higher than after the first one. This could be seen during first two consecutive compressions but no longer thereafter. Since the base was not moving upward at these points, it could be so that the factor capable of producing such force is the recovering compact. As the powder is compressed, the axial pressure is stored in radial direction and shortly thereafter released back in axial direction (Abdel-Hamid & Betz 2011; Hiestand et al. 1977). Due to momentum conservation principle, the collision between the recovering compact and the bar could thus cause an even higher rebound. This is logically possible since, at the time of the second impact, the position of the bar is lower than the final displacement level of the compact meaning that the collision between the bar and the recovering compact is inevitable. During further compressions, the springbacks after first impacts were higher and it took more time for the bar to reach the second

contact point. Therefore, it could be that the immediate compact recovery had already ended, resulting in a smaller second springback.

The energy spent on powder/further compact compression on each drop can be seen in Table 2. The energy spent on compact formation during the first compression of samples was calculated with the correlation method. It was found that during the first compression 9.2 J/g and 8.2 J/g was spent on compact formation, for MCC and starch respectively. Compaction pressure was 31.4 MPa for MCC and 60.1 MPa for starch. The result was close to a reference (approximately 9 J/g; 30 MPa for MCC and 7.5-13 J/g; 60 MPa for different starches) found in literature (Roopwani & Buckner 2011). One possible reason for the higher result for MCC could be that the compact remained inside the die and the calculations were based on distance data acquired immediately after the compression. Thus, the tablet inside the die was under constant stress and it would have recovered more of its volume had it been removed from the die (Abdel-Hamid & Betz 2011; Hiestand et al. 1977). The compact could have been left inside the die and the amount of recovery measured over time, but doing so could also increase the amount of plastic deformation in the compact and the result might be even less comparable to compression events where the tablets were immediately ejected. Furthermore, it is crucial to remember that all machines are unique in their features and working conditions vary.

Table 2: Energy spent on compact formation/further deformation in five consecutive compressions (n=3).

Non-elastic energy, other than that amount included in the compact formation (or internal energy of the compact) consists of machine deformation, vibration, friction, heat and sound (Buckner et al. 2010; Krok et al 2016; Stoianovici & Hurmuzlu 1996). Work is consumed and heat is released during powder deformation but some of this heat is reabsorbed during decompression phase. In this study, the amount of this energy is regarded relatively equal whether there is powder in the die or not. This, too, may cause error in the measurement, since one could assume that this relative amount is different

during collisions which are influenced by the properties of the powder. In this setting, measuring the amount of dissipated heat in each scenario would require a study of its own. During compression, heat is generated due to irreversible particle deformation, particle-particle and particle-die wall friction (Krok et al. 2016). This heat is then partially dissipated into the surroundings. However, this amount reduces when compression speed increases as the contact time between the powder and die wall remains short. In this work, contact time was less than 10 ms and compression speed was roughly 800 mm/s so it was assumed that, while acknowledging the possible source of error, the amount of dissipated heat during powder compaction was not too significant.

The results show that more energy was consumed in compact formation when compressing MCC which also supports the current knowledge of MCC being more compressible than starch (Shlieout 2002). However, the compression pressure varies between samples since the falling height (and thus total energy) is different and also since the material properties affect the magnitude of force on impact. However, while examining variation in compression pressures, differences in material compressibility can also be seen. Initially, when compressing MCC, lower pressure is required for a greater amount of energy to be consumed in powder compaction compared to starch compression. Pressure increases from 31.4 to 113.2 MPa for MCC and from 60.1 to 106.5 MPa for starch when compressed five times. This also indicates that MCC undergoes more change during compressions as the pressure increases more drastically when compared to starch compressions. Also, it is of importance to notice that before first compression the sample is in powder form and after that in compact form. This dramatically affects how the compaction pressure changes after the first compression. However, this method could also be utilized in cases where the sample remained in powder form or very weak compact form throughout compressions.

Properties of compacts formed by this method have not yet been studied. So far, the aim has been to prove that the method is valid for powder compression examination. Also, the actual simulating capabilities when compared to tablets produced with tableting machines remain unknown at the moment. Furthermore, compression speed in this study was roughly 800 mm/s but it can be remarkably increased when necessary. With this method, compression speed depends on the falling

height and thus the effects of speed can be analyzed by changing the punch/die diameter and the weight of the bar to balance the compression pressure. In the end, even the pressure adjustment can only be done roughly since the powder properties ultimately determine the compaction pressure. Thus, resulting compact volume and compaction pressure, which are usually more or less predetermined values in a typical tableting setting, are actually results in the gravitational analysis.

5. CONCLUSIONS

In conclusion, the gravitation-based high-velocity compaction analysis method can be utilized to examine powder compression phenomena in a cost-efficient and elementary manner. The method is unique in a way that the properties of powder itself determine the impact force, springback height and displacement levels, without forcing the compact into a predetermined volume. Due to the 20 kHz sampling rate and 1 μm detection resolution, the method was proven to be both accurate and reproducible, despite the high vertical compression speed, which is imperative for the method to be functional. With the method, merely distance measurement with a known sampling frequency is necessary as it can be derived to obtain velocity, kinetic energy, acceleration, maximum force on impact and energy spent on powder compaction. The present study shows that high-velocity gravitational compaction analysis is a suitable platform to provide unique and novel information of the compression properties of granular material.

Acknowledgements

We would like to kindly acknowledge Heikki Räikkönen (Faculty of Pharmacy, University of Helsinki) for technical assistance.

Conflicts of interest

None

References

Abdel-Hamid S. & Betz G. 2011: Study of radial die-wall pressure changes during pharmaceutical powder compaction—Drug Dev. Ind. Pharm. 37: 387-395

Adolfsson Å. & Nyström C. 1996: Tablet strength, porosity, elasticity and solid state structure of tablets compressed at high loads—Int. J. Pharm. 132: 95-106

Amidon G.E. & Houghton M.E. 1995: The effect of moisture on the mechanical and powder flow properties of microcrystalline cellulose—Pharm. Res. 12: 923-929

Antikainen O. & Yliruusi J. 2003: Determining the compression behaviour of pharmaceutical powders from the force-distance compression profile—Int. J. Pharm. 252: 253–261

Buckner I.S., Friedman R.A. & Wurster D.E. 2010: Using compression calorimetry to characterize powder compaction behavior of pharmaceutical materials—J. Pharm. Sci. 99: 861-870

Haware R.V., Tho I. & Bauer-Brandl A. 2010: Evaluation of a rapid approximation method for the elastic recovery of tablets—Powder Technol. 202: 71-77

Hiestand E.N., Wells J.E., Peot C.B. & Ochs J.F. 1977: Physical processes of tableting— J. Pharm. Sci. 66: 510–519

Katz J.M., Roopwani R. & Buckner I.S. 2013: A material-sparing method for assessment of powder deformation characteristics using data collected during a single compression-decompression cycle—J. Pharm. Sci. 102:3687–3693

Kremer D.M. 2006: A numerical investigation of air flow during tablet compression—Chem. Eng. Sci. 61: 7963–7978

Krok A., Mirtic A., Reynolds G.K., Schiano S., Roberts R. & Wu, C.-Y. 2016: An experimental investigation of temperature rise during compaction of pharmaceutical powders—Int. J. Pharm. 513: 97-108

Michaut F., Busignies V., Fouquereau C., Huet De Barochez B., Leclerc B. & Tchoreloff P. 2010: Evaluation of a rotary tablet press simulator as a tool for the characterization of compaction properties of pharmaceutical products—J. Pharm. Sci. 99: 2874-2885

Neuhaus T. 2007: Investigation and Optimisation of the Presster-A Linear Compaction Simulator for Rotary Tablet Presses—PhD Thesis, Bonn, Germany—*Available online at* http://hss.ulb.uni-bonn.de/2007/1152/1152.pdf—09.11.2016

Nokhodchi A. 2005: An overview of the effect of moisture on compaction and compression—Pharm. Technol. 29: 46–66

Rees J.E., Hersey J.A. & Cole T.E. 1972: Simulation Device for Preliminary Tablet Compression Studies—J. Pharm. Sci. 61: 1313-1315

Roopwani R. & Buckner I.S. 2011: Understanding deformation mechanisms during powder compaction using principal component analysis of compression data—Int. J. Pharm. 418: 227– 234

Rouèche E., Serris E., Thomas G. & Périer-Camby L. 2006: Influence of temperature on the compaction of an organic powder and the mechanical strength of tablets—Powder Technol. 162: 138–144

Shlieout G., Laich T. & Zessin G. 2002: Evaluating the Elastic Behavior of
485 Pharmaceutical Excipients and Binary Mixtures Using the Modified Fraser-Suzuki Function—Pharm. Technol. Eur. 14: 21–28

Stoianovici, D. & Hurmuzlu, Y. 1996: A critical study of the applicability of rigid body collision theory—J. Appl. Mech. 63: 307-316

490

Tatavarti S.A., Muller F.X., & Hoag S.W. 2008: Evaluation of the deformation behavior of binary systems of methacrylic acid copolymers and hydroxypropyl methylcellulose using a compaction simulator—Int. J. Pharm. 348: 46-53

495 Thoorens G., Krier F., Leclercq B., Carlin B & Evrard B. 2014: Microcrystalline cellulose, a direct compression binder in a quality by design environment—A review—Int. J. Pharm. 473: 64-72

Zhang Y., Law Y. & Chakrabarti S. 2003: Physical Properties and Compact Analysis of Commonly Used Direct Compression Binders—AAPS PharmSciTech 4: 489-499

500

Table 1
Sample and compact characteristics (average ± standard deviation; n = 3).

T = 25–26 °C; R.H. = 32-33% (ambient)	Before compression			After compression		
Excipient	Water activity	Sample mass (mg)	Powder bed height (mm)	Out-of die tablet height (mm)	Out-of-die tablet width (mm)	Compact mass (mg)
MCC	0.228 ± 0.013	200.0 ± 0.2	7.757 ± 0.155	3.033 ± 0.031	8.326 ± 0.022	198.4 ± 1.7
Starch	0.215 ± 0.007	200.3 ± 0.1	5.690 ± 0.014	3.457 ± 0.016	8.269 ± 0.004	192.3 ± 1.2

Table 2
Energy spent on compact formation/further deformation in five consecutive compressions (n = 3).

MCC Compression no	Etotal (J)	Epowder (J/g)	Epowder (%)	Pressure (MPa)
1	2.220 ± 0.002	9.20 ± 0.04	82.9 ± 0.3	31.4 ± 0.3
2	2.259 ± 0.002	8.55 ± 0.01	75.7 ± 0.2	61.4 ± 0.9
3	2.279 ± 0.002	8.19 ± 0.04	71.9 ± 0.4	87.7 ± 1.2
4	2.291 ± 0.002	7.71 ± 0.06	67.4 ± 0.6	103.0 ± 0.9
5	2.298 ± 0.002	7.13 ± 0.09	62.1 ± 0.8	113.2 ± 1.3
Starch Compression no	**Etotal (J)**	**Epowder (J/g)**	**Epowder (%)**	**Pressure (MPa)**
1	2.256 ± 0.001	8.18 ± 0.05	72.5 ± 0.4	60.1 ± 1.3
2	2.272 ± 0.001	7.64 ± 0.01	84.1 ± 0.0	84.4 ± 1.3
3	2.279 ± 0.001	7.34 ± 0.05	64.4 ± 0.4	95.5 ± 0.7
4	2.284 ± 0.001	7.01 ± 0.05	61.4 ± 0.4	102.0 ± 0.9
5	2.287 ± 0.001	6.77 ± 0.05	59.2 ± 0.5	106.5 ± 1.1

Fig. 1

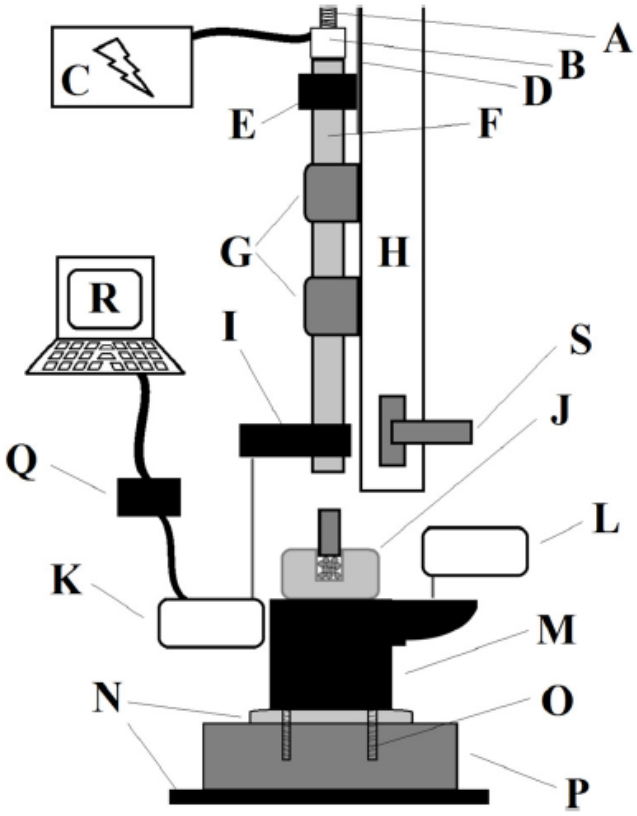

505 Fig. 2

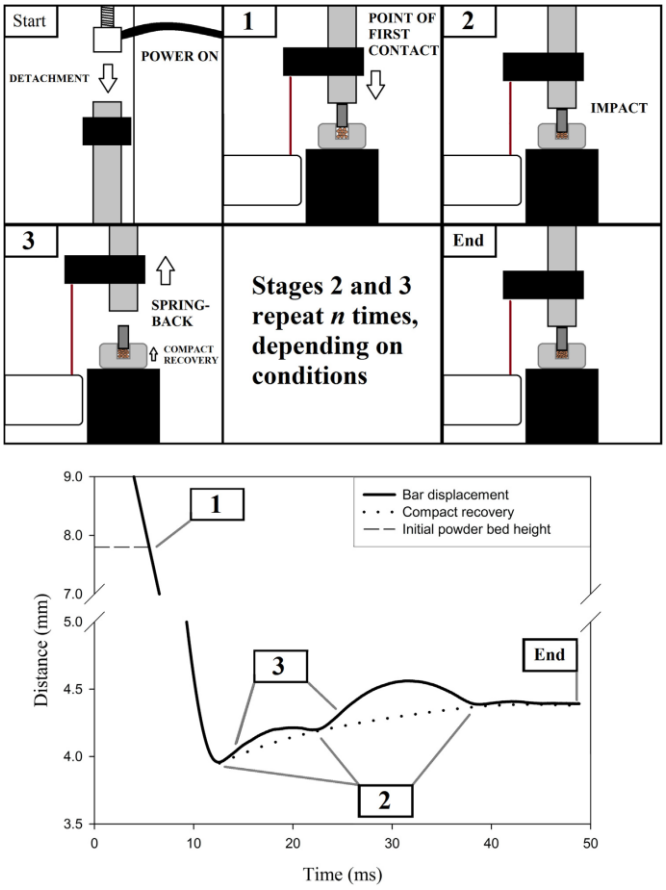
Start
POWER ON
DETACHMENT
1
POINT OF FIRST CONTACT
2
IMPACT
3
SPRING-BACK
COMPACT RECOVERY
Stages 2 and 3 repeat n times, depending on conditions
End
Bar displacement
Compact recovery
Initial powder bed height
Distance (mm)
Time (ms)

Fig. 3

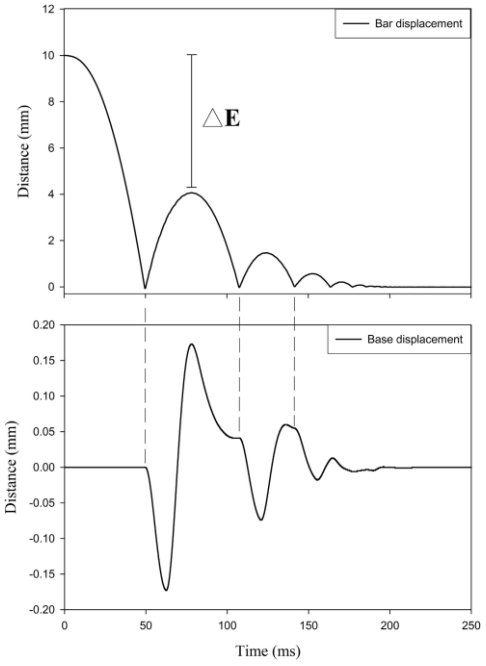
Bar displacement
△E
Distance (mm)
Base displacement
Distance (mm)
Time (ms)

Fig. 4

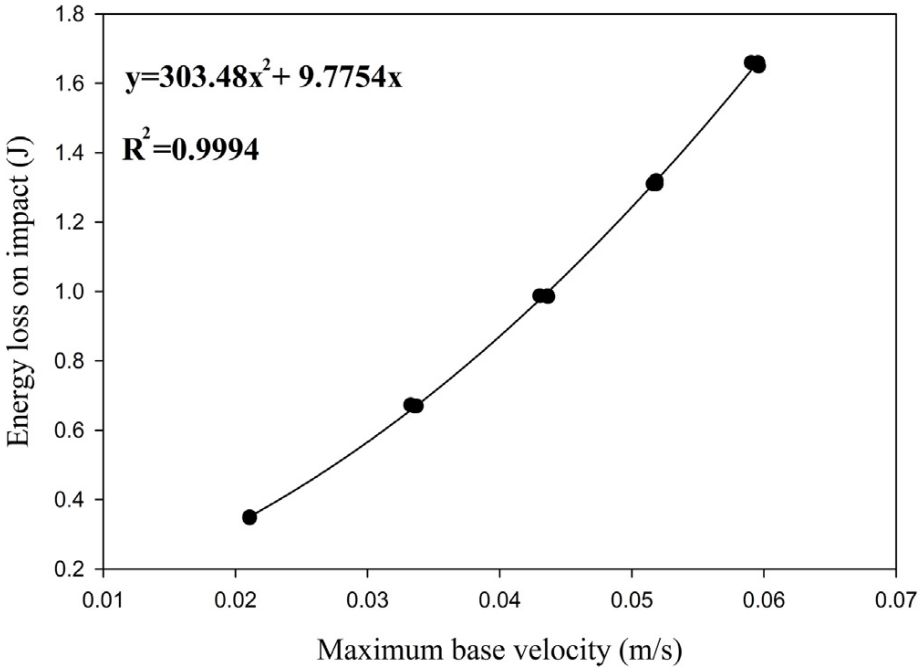

510

Fig. 5

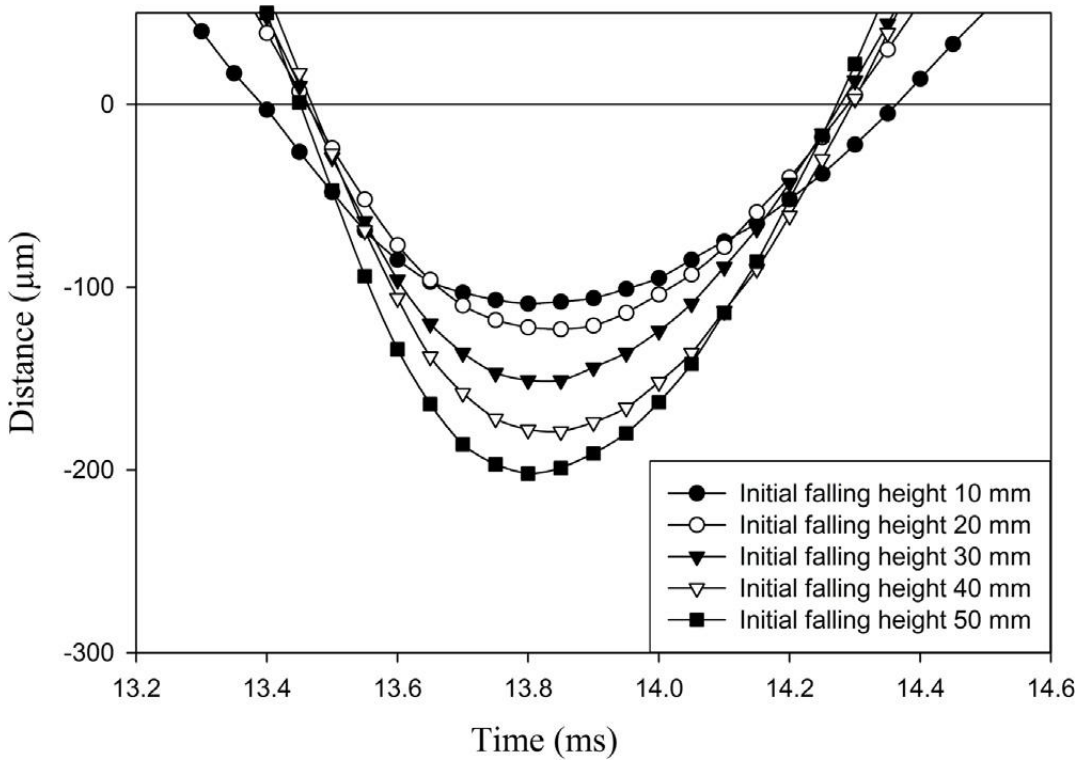

515

Fig. 6

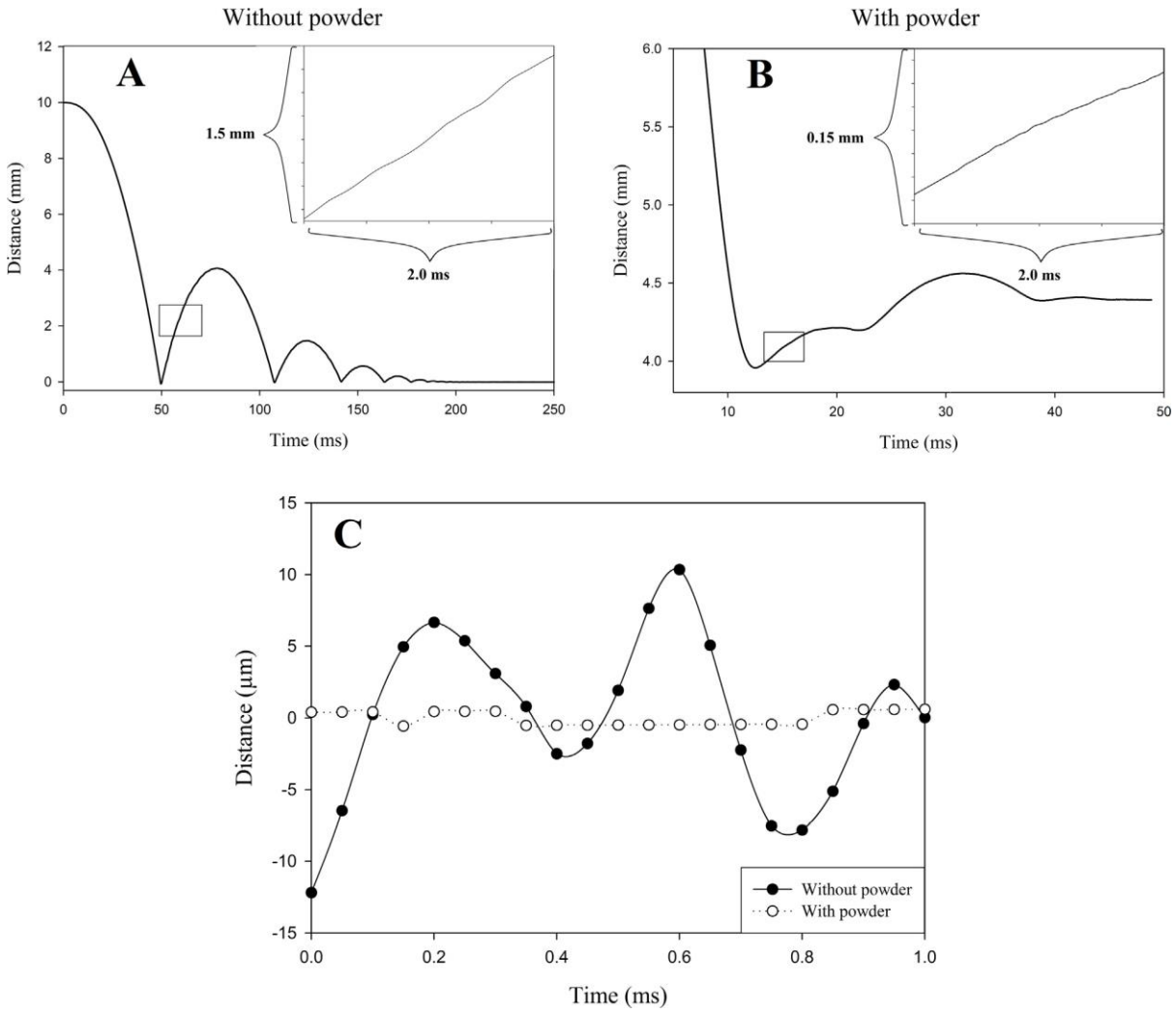
Without powder
With powder
A
B
C
1.5 mm
2.0 ms
0.15 mm
2.0 ms
Distance (mm)
Time (ms)
Distance (μm)
Without powder
With powder

520

525 Fig. 7

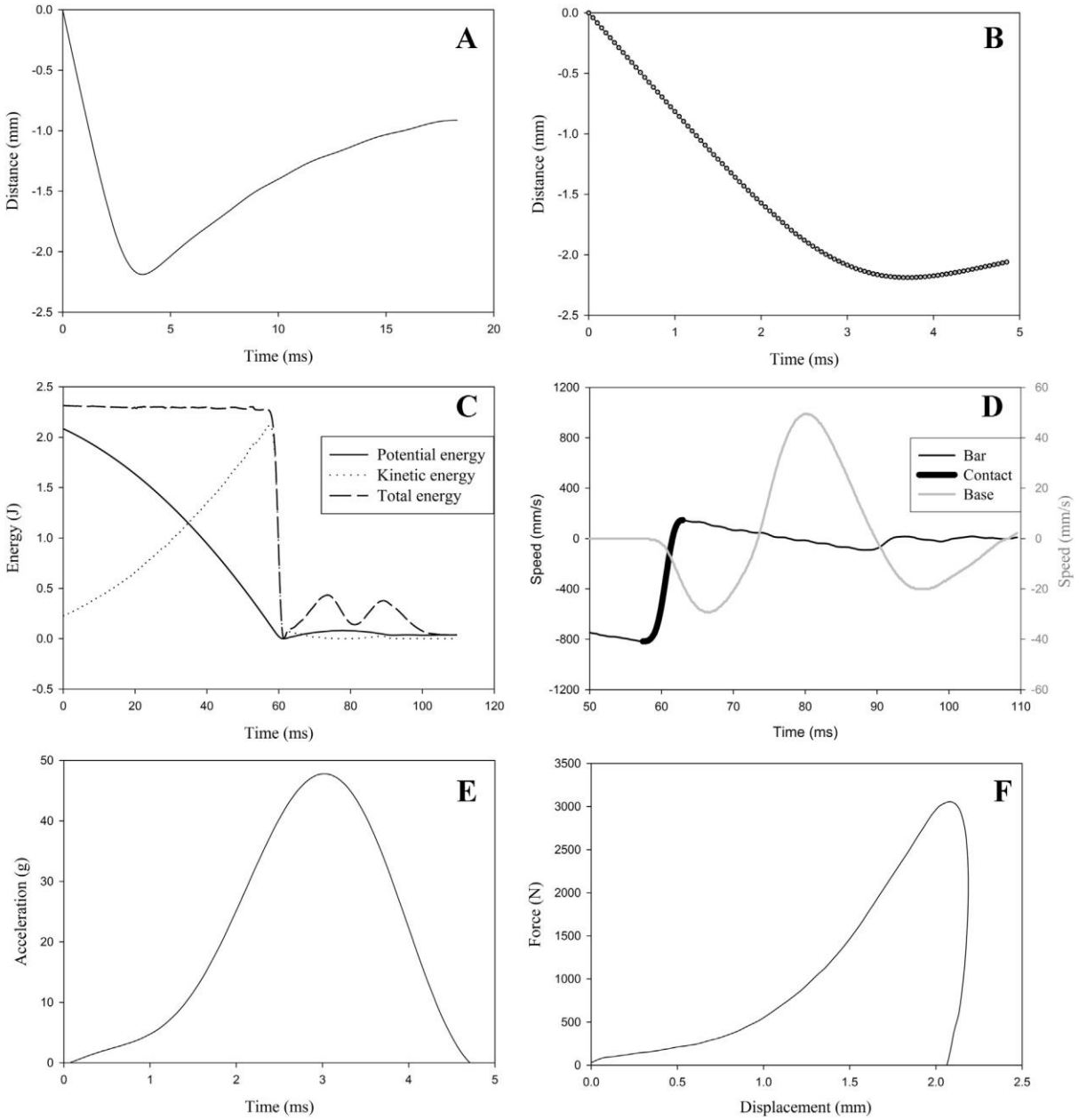
A
Distance (mm)
Time (ms)
B
Distance (mm)
Time (ms)
C
Potential energy
Kinetic energy
Total energy
Energy (J)
Time (ms)
D
Bar
Contact
Base
Speed (mm/s)
Speed (mm/s)
Time (ms)
E
Acceleration (g)
Time (ms)
F
Force (N)
Displacement (mm)

530

Fig. 8

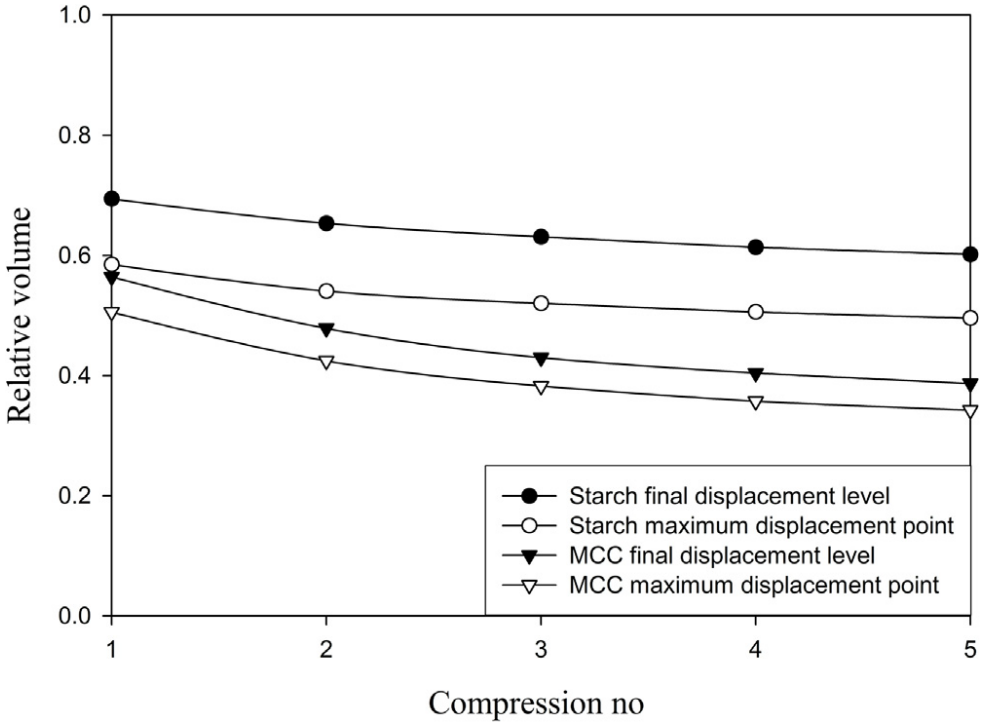
1.0
0.8
0.6
0.4
0.2
0.0
Relative volume
1
2
3
4
5
Compression no
Starch final displacement level
Starch maximum displacement point
MCC final displacement level
MCC maximum displacement point

Fig. 9

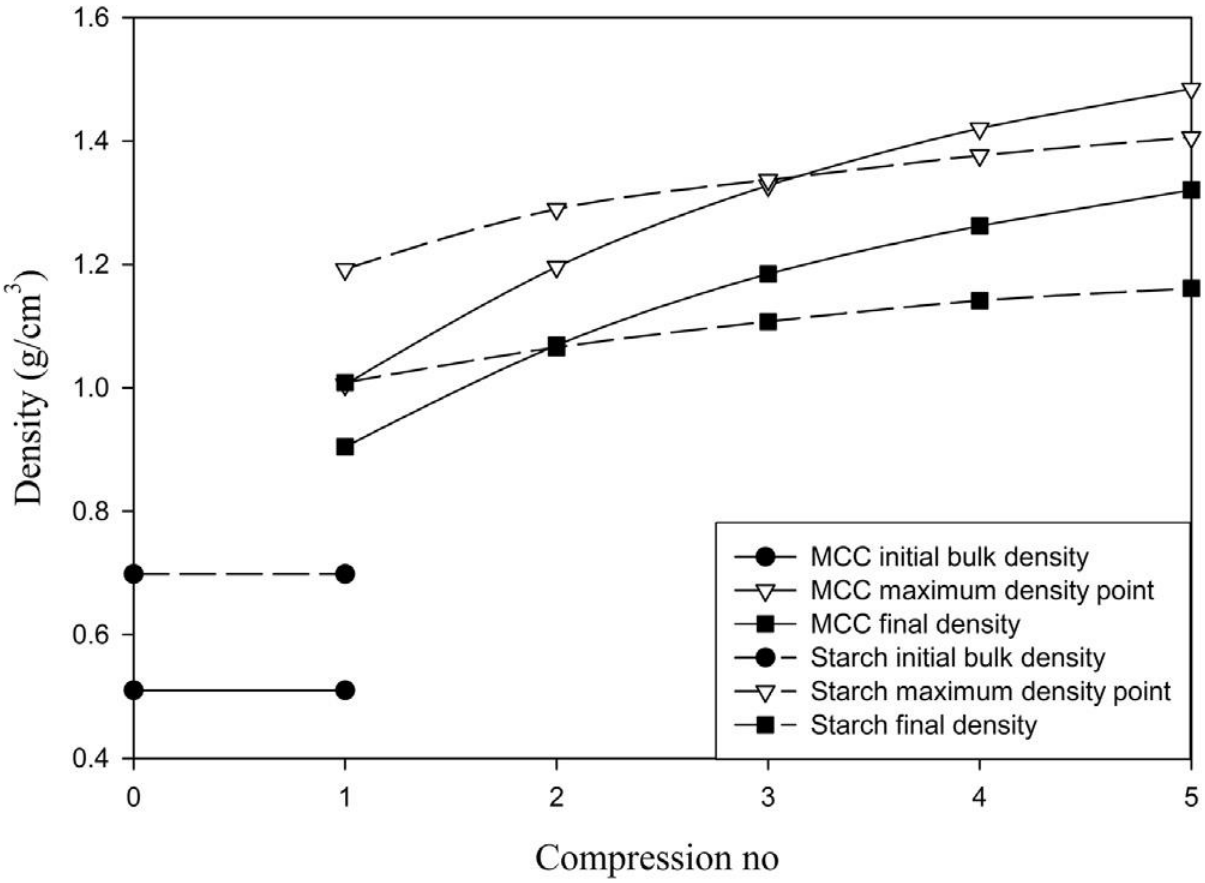
1.6
1.4
1.2
1.0
0.8
0.6
0.4
Density (g/cm3)
0
1
2
3
4
5
Compression no
MCC initial bulk density
MCC maximum density point
MCC final density
Starch initial bulk density
Starch maximum density point
Starch final density

535